INTL JOURNAL OF ELECTRONICS AND TELECOMMUNICATIONS, 2022, VOL. 68, NO. 2, PP. 267-273
Manuscript received January 1, 2022; revised May, 2022. DOI: 10.24425/ijet.2022.139877

Millimeter-Wave Transmitter with LTCC Antenna and Silicon Lens

Paweł Bajurko, Jakub Sobolewski, Grzegorz Bogdan, Konrad Godziszewski, Jacek Marczewski, Jan Kulawik, Michał Widlok, and Yevhen Yashchyshyn

***Abstract*—Millimeter-wave (mm-wave) transmitters are often fabricated using advanced technology and require a sophisticated manufacturing facility. Access to such technologies is often very limited and difficult to gain particularly at the initial stage of research. Therefore, to increase the accessibility of mm-wave transmitters, this study proposes a design that can be assembled in a standard microwave laboratory from commercially available or externally ordered components. The transmitter demonstrated in this paper operates above 100 GHz and is based on a low-temperature co-fired ceramic board in which the antenna array, microstrip lines, and power-supply lines are fabricated in a single process. Different technologies are used to assemble the module, e.g., wire-bonding, soldering, and wax adhesion. Advantages and disadvantages of the proposed design are given based on experimental evaluation of the prototype. Although the performance of the developed transmitter is not as good as that of the similar modules available in the recent literature, the results confirm the feasibility of a mm-wave transmitter that is assembled without employing advanced technologies and superior machinery.**

***Keywords*—antenna-in-package; LTCC circuits and modules; millimeter-waves; RF modules; RFIC and MMIC packaging; silicon lenses**

I. Introduction

SYSTEM-IN-PACKAGE transceivers are essential for ubiquitous implementation of millimeter-wave (mm-wave) communication devices. The integration of fundamental building blocks (e.g., amplifiers, frequency multipliers, frequency converters, and antennas) has significantly increased over the last two decades [1]–[3]. However, the integration of directional antenna arrays in mm-wave modules with frequencies above 100 GHz remains an interesting topic for further research [4]–[7]. The two most popular methods for integration of components and antenna into a complete self-contained module are the antenna-on-chip (AoC) and antenna-in-package (AiP) methods.

This work was supported by The National Center for Research and Development (NCBiR) in Poland, contracts no. PBS3/A3/18/2015 and PBS3/B3/30/2015.

P. Bajurko, J. Sobolewski, G. Bogdan, K. Godziszewski and Y. Yashchyshyn are with the Warsaw University of Technology, Institute of Radioelectronics and Multimedia Technology, Warsaw, Poland (e-mail: {P.Bajurko; J.Sobolewski; K.Godziszewski; G.Bogdan; Y.Yashchyshyn}@ire.pw.edu.pl).

J. Marczewski and J. Kulawik are with the Łukasiewicz Research Network, Institute of Microelectronics and Photonics, Warsaw, Poland (e-mail: {jacek.marczewski; jan.kulawik}@imif.lukasiewicz.gov.pl).

Michał Widlok is with the SIRC Sp. z o.o., Gdynia, Poland (e-mail: m.widlok@si-research.eu).

In the AoC approach, the antenna is integrated directly in a semiconductor die; thus, no high frequency interconnections are required [6]–[8]. However, the antenna gain is limited because the chip area is confined. Another drawback of the AoC is the antenna-performance deterioration because of the unfavorable electrical properties of the semiconductor substrate (i.e., low resistivity and high permittivity).

The AiP concept provides more flexibility in the design because the antenna can occupy a larger area and can be fabricated on a substrate whose electrical parameters are tailored for better antenna performance [9]. Typical substrates used in the mm-wave AiP include the following: polymer [10], highly resistive silicon [11], ceramic-filled polytetrafluoroethylene (PTFE) composites [4], organic resin laminates [5], quartz [12], and low-temperature co-fired ceramics (LTCC) [13]. The last substrate type is a leading thick-film technology for AiP. It can be used to manufacture robust integrated modules and components suitable for use in applications demanding high performance and reliability, such as automotive, telecommunication, aviation and space. Nowadays, LTCC can be also found in mass produced components, particularly in multilayer capacitors and miniature antennas. It is also used in integrated mm-wave modules that operate up to 80 GHz [14]–[17]. Although many designs of LTCC antennas that operate above 80 GHz have been published, e.g., 94 GHz [18], 122 GHz [19], 130 GHz [20], 140 GHz [21], 159 GHz [22], 270 GHz [23], and 300 GHz [24], these antennas were not integrated in a mm-wave device. Only a few integrated devices that comprise LTCC antennas operating at these frequencies have been demonstrated [25]. The crucial problem of integrating LTCC antennas with transceiver chips is the interconnection loss. Wire bonds, which are commonly used as interconnects in microelectronics, introduce large transmission loss and reflection loss which increases substantially with the frequency, making them virtually unusable at frequencies above 60 GHz. Therefore flip chip [26] or ribbon bonds [27] are often used instead. Nevertheless, the recent study shows, that the wire bonding mounting technology is suitable for integration of mm-wave components when applied with an adequate manner, for example with consideration of a proper matching circuit [28]. In [29] wire bonds are successfully used in a 122-GHz silicon-germanium radar transceiver chip for integration in LTCC-based package by taking into consideration: the typical LTCC manufacturing defects, self-compensation of wire bonds, and a standard molding compound-based encapsulation methodology.

TABLE I
OVERVIEW OF MM-WAVE TRANSMITTERS (TX) AND TRANSCEIVERS (TX/RX) INTEGRATED WITH ANTENNA AND LENS

Frequency	Type	Integration	Substrate	Antenna type	Type of lens	Material of lens	EIRP/Gain	Ref
78 GHz	Tx	AiP	eWLB	two-element patch antenna array	Hemispheric rod	PEEK polymer	18.5 dBm / >12dBi	[31]
122 GHz	Tx/Rx	AoC	Silicon	Circularly polarized slot antenna	n/a	High-resistivity silicon	n/a / 16 dBi	[6]
130 GHz	Tx/Rx	AiP	RO3003	Differential patch antenna	Hyper-hemispherical	Polyamide	n/a / 21.5 dBi	[4]
130 GHz	Tx/Rx	AiP	Organic	2×2 slot-fed patch antenna array	Elliptical dome	ABS-M30	33 dBm / 28 dBi	[5]
180 GHz	Tx	AoC	Silicon	Dipole antenna	Hyper-hemispherical	High-resistivity silicon	n/a / 17.2 dBi	[7]
300 GHz	Tx	AiP	PCB/Quartz	Stacked patch	Elliptical	HDPE	20 dBm / 23 dBi	[12]
420 GHz	Tx	AoC	SiGe	8×8 circular slot antenna array	Hyper-hemispherical	Silicon	Power: 10.3 dBm	[8]

Although integrated LTCC devices that operate even at frequencies higher than 300 GHz can be found in the literature, they do not use LTCC antennas. For example, in [30] the antenna of LTCC-based transmitter that operates at 312 GHz is integrated as AoC.

Both AoC and AiP are often complemented with a dielectric lens. This concept allows to obtain a relatively high gain (as high as 28 dBi [5]) without a large antenna. Antennas used together with lens are typically patch antennas [5, 31], however, slot [6, 8] and dipole [7] antennas are also suitable. The lens is usually made of silicon [8], high-resistive silicon [6,7], polyamide [4], polyether ether ketone (PEEK) polymer [31], or high density poly ethylene (HDPE) [12]. Comparison of AoC designs is given in Table I.

In this paper, we present a mm-wave AiP transmitter that operates above 100 GHz and is composed of a two-element antenna array on an LTCC substrate, a monolithic microwave integrated circuit (MMIC), and other components integrated into a single package. The antenna performance is enhanced with the application of a silicon lens.

This paper is organized as follows: Section II describes the transmitter design; Section III presents the measurements of the manufactured device; finally, Section IV provides the conclusions.

II. TRANSMITTER DESIGN

A general diagram of the transmitter design is shown in Fig. 1. It is composed of the front-end MMIC, matching circuit, antenna array, LTCC board, and silicon lens. These elements are either custom designs or commercially available off-the-shelf (COTS) components.

A. MMIC

The main functions of the MMIC are to multiply the frequency of the external local oscillator (LO) signal by eight and amplify its power to compensate the conversion loss. The MMIC is realized in a silicon-germanium (SiGe) technology (SG13S SiGe:C BiCMOS process by IHP) and comprises four main blocks:

- Balun (single-ended to differential) at the input
- Frequency multiplier (×8) composed of three stages of frequency doublers in which each has a resonant output circuit (all stages are identical, however, with individual frequency tuning)
- Balun (differential to single-ended)
- Power amplifier (PA) at the output.

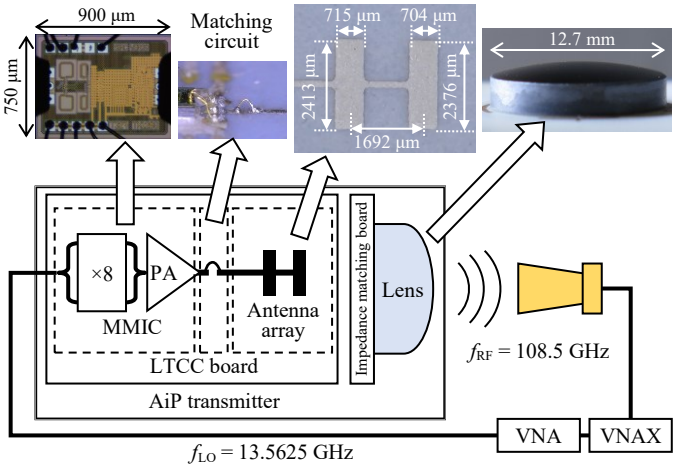

Fig. 1. General diagram of transmitter with experimental setup

The design of power amplifier is based on three-stage cascode topology with impedance matching circuits at input and output. Each amplifier stage is built with bipolar transistors. The main advantage of cascode design is minimized influence of parasitic capacitances of transistors. It is widely used in bipolar RF amplifier ICs. Output of the amplifier is matched to 50 Ω.

Five MMIC samples were measured on-wafer using probe-station measurement setup to determine their characteristics and output-power spread [32]. The measurement results are shown in Fig. 2. The power of the input signal at frequency f_{LO} swept in a range from 11.25 to 17.5 GHz was set to −5 dBm. The maximum power level measured at the MMIC output was −12.7 ± 2 dBm at frequency f_{RF} = 108.5 GHz.

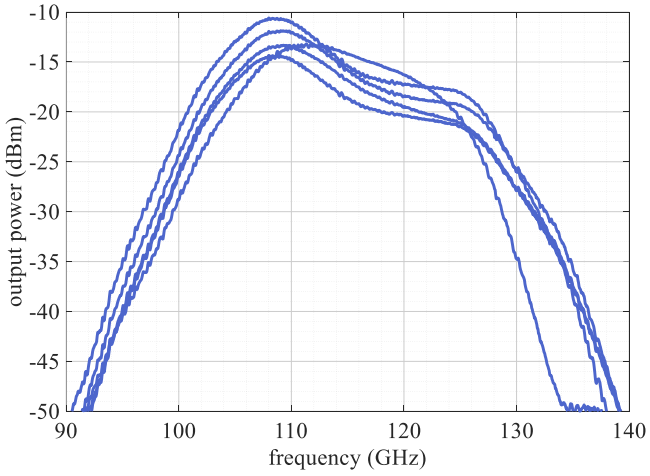

Fig. 2. Measured output power of MMIC (five samples tested) [32]

B. Matching Circuit

The MMIC was connected to the circuit on the LTCC board using bond wires (Fig. 1). To compensate the bond-wire inductance at the MMIC output, an LCL (inductance-capacitance-inductance) interconnect matching circuit was used [29]. This circuit is constructed by introducing an additional pad between MMIC and antenna feed line serving as a capacitor and connecting it with bond wires on both sides serving as inductive components.

C. Antenna Array

The designed antenna array is composed of two series-fed patch antennas. A photograph that illustrates the dimensions of the antenna array is shown in Fig. 1. A 70-µm thick (fired) 41110-T LTCC foil from ESL ElectroScience was used as a substrate. This material is suitable for microstrip antennas because of its low permittivity ($\varepsilon_r = 4.05$) and low loss tangent ($tg\delta = 0.006$) at mm-wave frequencies [33] as well as negligible firing shrinkage in the plane parallel to the patch [34].

D. LTCC Board

The LTCC board is shown in Fig. 3. It is made of two layers of 70-µm-thick LTCC foil placed on the top of a 0.5-mm-thick alumina plate. The middle ground plane separates the two LTCC layers. Therefore, only a single layer accounts for the design of the antenna array and 140-µm-wide microstrip antenna feedline. The second transmission line interconnects the MMIC and coaxial connector. This line requires a thicker substrate than the antenna array to match the microstrip line width with the diameter of the coaxial connector center pin and simultaneously maintain a 50 Ω impedance. Therefore, the middle ground plane has a cutout, which doubles the thickness of the LTCC substrate under the line.

To connect the wide microstrip line near the coaxial connector to a narrow line near the MMIC, a special transition is designed and applied at the edge of the ground plane cutout to achieve line-impedance continuity [35].

Conductive walls are buried along the perimeter of the middle ground plane and along the cutout edges to provide a good electrical connection between the two ground planes and coaxial connector. This solution achieves better high frequency performance than typical vias due to lower inductance and resistance of conductive walls. The bonding pads are coated with gold paste to provide compatibility with the gold bonding wires. Besides high frequency connections, LTCC board is used for MMIC power supply connections with local decoupling.

E. Lens

A high-resistivity silicon plano-convex lens with a diameter of 12.7 mm, thickness of 3 mm, and curvature radius of 23.77 mm is suspended over the antenna array (Fig. 4) to focus the beam, hence increasing the EIRP. The lens is attached using a thin layer of wax adhesive to an impedance matching board made of a 0.305-mm-thick Rogers RO4003C microwave substrate ($\varepsilon_r = 3.55$). The matching board constitutes a quarter-wave impedance transformer that provides impedance matching between the silicon and air at the planar surface of the lens. The convex surface of the lens was not covered by the transformer layer due to technological difficulties in applying such a layer to non-planar surface. Therefore it can still introduce some reflections. Fig. 5 shows the comparison of the field distributions of the plane wave incident to the convex surface of the silicon lens with (Fig. 5a) and without (Fig. 5b)

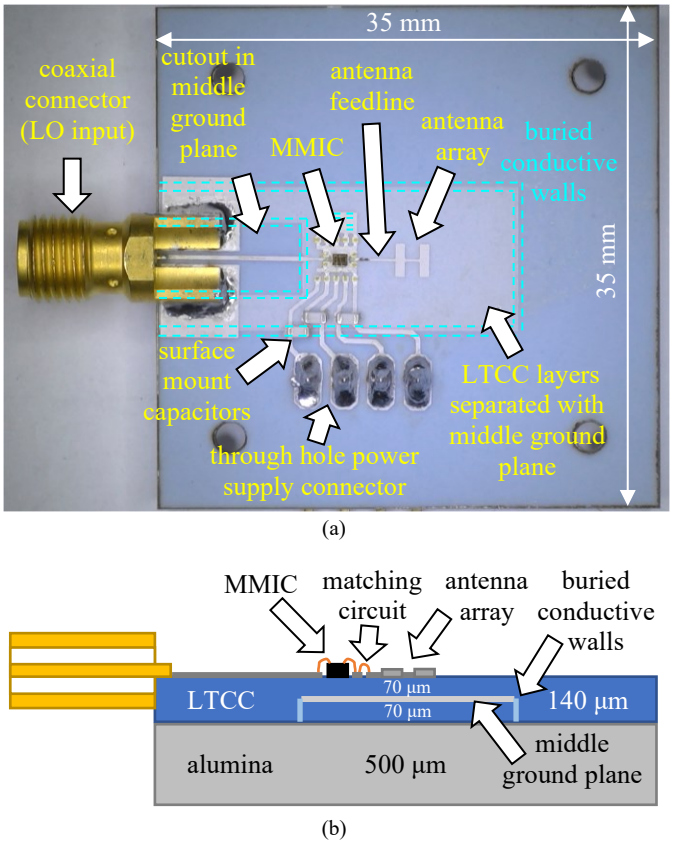

Fig. 3. LTCC board: (a) Top view; (b) Side view (cross-section, not to scale)

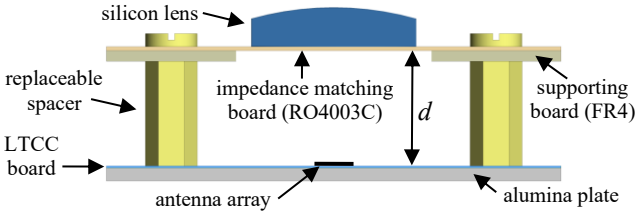

Fig. 4. Model of adjustable fixture (side view)

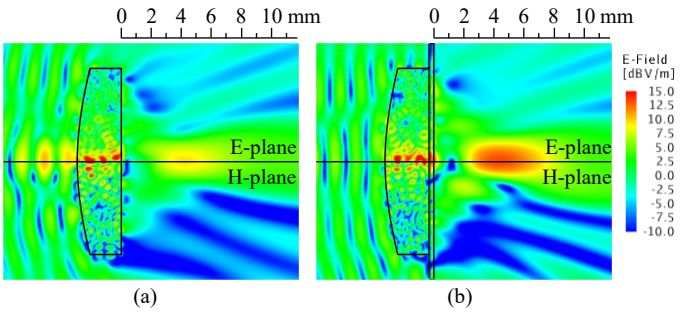

Fig. 5. Electromagnetic simulation of the electric field magnitude distribution of a plane wave approaching from the left side (0 dBV/m amplitude). (a) Wave propagating through the silicon lens without an impedance matching board. (b) Wave propagating through the silicon lens with an impedance matching board.

the impedance matching board at 108.5 GHz. The field distributions were calculated using MLFMM method implemented in Altair FEKO electromagnetic simulator. As it can be observed, the transformer significantly reduces the reflections from the lens and increases the electric field intensity at the focal point. The transformer board also serves as a mechanical suspension for the lens. In addition, a supporting board made of glass-reinforced epoxy laminate (FR4) is used to increase the construction stability.

Distance d between the matching board and antenna array (Fig. 4) can be adjusted using replaceable spacers for fine tuning of the focus. The nominal focal length of the lens determined from the geometrical optics principles equals 9.8 mm. However, as can be seen in Fig. 5, the maximum of the electric field distribution is located in the closer distance, at 4.3 mm in both cases with and without the impedance transformer. This discrepancy results from a strong spherical aberration of spherical lens coinciding with diffraction effects. The beam focus zone is elongated, therefore the tolerance of the distance between lens and antenna array is high. However, the space confined by LTCC board and lens can form a parallel-plate resonator (the effect not shown in Fig. 5). In that case the distance d will have to be precisely adjusted to achieve maximal transmitter performance.

III. Measurements

The assembled transmitter module is shown in Fig. 6. The module was measured according to the setup shown in Fig. 1. The instruments used in the measurements included the Agilent Technologies PNA-X N5245A vector network analyzer (VNA), VDI WR8 waveguide frequency extender (VNAX), a high-gain horn antenna, and a programmable rotary table. Both the device under test and the frequency extender with the horn antenna were mounted on the precision positioning devices allowing accurate alignment. Distance between the antennas (1.04 m) were chosen to fulfill far field measurement condition. VNA serves as a tunable generator of LO signal (13.125 GHz < f_{LO} < 14.125 GHz) as well as a receiver of a mm-wave signal (105 GHz < f_{RF} < 113 GHz), which is down-converted by VNAX. The EIRP of the transmitter is determined from the link budget of the experimental setup, i.e.,

$$\mathrm{EIRP} = P_{\mathrm{Rx}} - G_{\mathrm{VNAX}} - G_{\mathrm{Rx}} + L_{\mathrm{FS}}, \qquad (1)$$

where P_{Rx} denotes the level of power recorded in the internal VNA receiver, G_{VNAX} is the VNAX conversion gain, G_{Rx} is the receiving antenna gain, and L_{FS} is the free-space loss.

The EIRP measured when lens distance d was varied from 3 to 8.5 mm at a frequency of 108.5 GHz is shown in Fig. 7. The EIRP fluctuated with the lens distance at a period of approximately 1.4 mm (half of the wavelength). Despite the application of the impedance transformer to the planar surface of the lens, the convex surface could still cause reflections, resulting in the observed effect. This result indicates that the adjustable fixture formed a type of parallel-plate resonator. Therefore, the distance needs to be precisely adjusted to achieve optimal performance (with approximately 0.1 mm

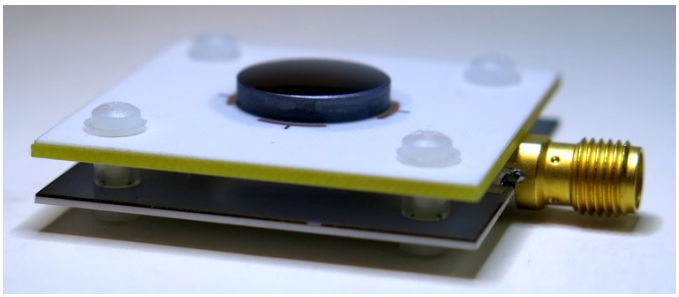

Fig. 6. Assembled transmitter module

precision). The highest EIRP (−3.8 dBm) was obtained at d = 3.84 mm. This distance was used for further measurements. It can be noticed that the distance of maximum EIRP corresponds well to the lens focal point distance from Fig. 5b. Also the consecutive maxima in Fig. 7 are only slightly weaker than the first one, which reflects elongated beam focus zone visible in Fig. 5b.

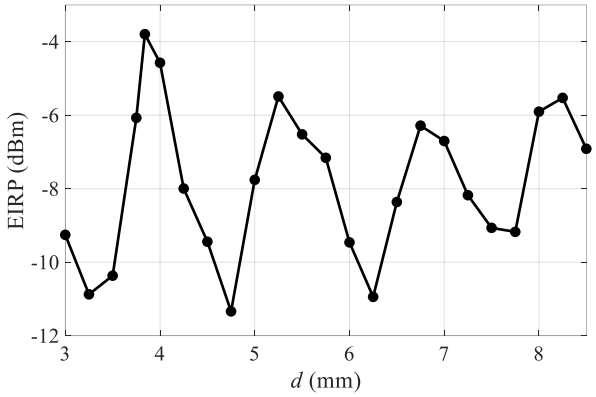

Fig. 7. EIRP versus distance d measured at 108.5 GHz

The frequency characteristics of the EIRP for the transmitter module with and without the lens are shown in Fig. 8. The highest EIRP value of −3.8 dBm was measured for the transmitter with the lens at 108.5 GHz. The 3-dB bandwidth of the device equals 2.2 GHz (from 107.5 to 109.7 GHz). The application of the lens has improved the EIRP by approximately 10 dB compared with that in the module without the lens.

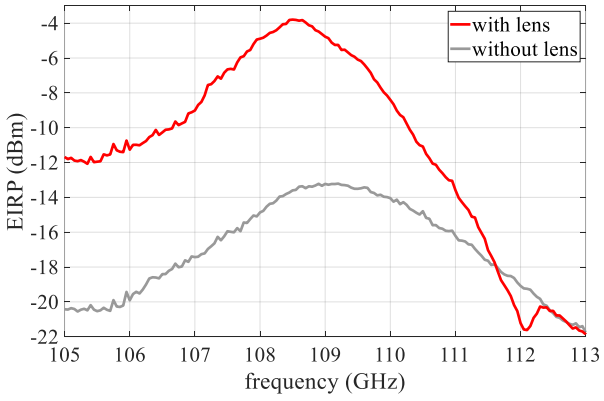

Fig. 8. Measured EIRP versus frequency

TABLE II
OVERVIEW OF TRANSMITTERS (TX) AND TRANSCEIVERS (TX/RX) THAT EMPLOY AIP ON LTCC SUBSTRATES

Frequency	Type	Antenna type	MMIC Type	Interconnect	Lens	EIRP	Ref
60 GHz	Tx	two-element patch antenna array	OOK modulator	wire bonding + matching circuit	No	10.7 dBm	[37]
60 GHz	Tx/Rx	2×2 patch antenna array	amplifiers, oscillator and mixers	flip chip	No	11.6 dBm	[38]
79 GHz	Tx/Rx	grid array antennas	radar front-end	wire bonding + matching circuit	No	13.1 dBm	[15]
79 GHz	Tx/Rx	10×1 and 10×3 patch antenna arrays	radar front-end	flip chip	No	n/a	[16]
79 GHz	Tx/Rx	5×1 patch antenna arrays	radar front-end	wire bonding + matching circuit	No	n/a	[17]
90 GHz	Tx	four-element patch antenna array	phase shifters, amplifiers and mixer	flip chip	No	10.6 dBm	[39]
122 GHz	Tx/Rx	6×6 mushroom antenna arrays	radar front-end	λ/2 wire bonding	No	n/a	[29]
108.5 GHz	Tx	two-element patch antenna array	multiplier and amplifier	wire bonding + matching circuit	Yes	−3.8 dBm	this work

The radiation patterns measured at the frequency of 108.5 GHz are shown in Fig. 9. The lens narrowed the beam in both E- and H-planes. The 3-dB beamwidth was equal to 15.5° in the E-plane and 15° in the H-plane. According to [36], the directivity estimated on the basis of the beamwidths equals 22.5 dBi.

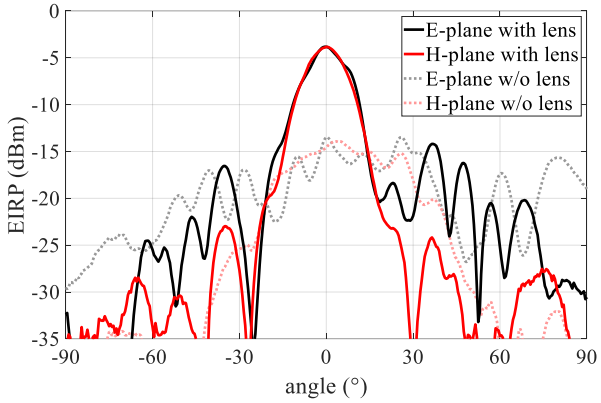

Fig. 9. Radiation patterns measured at 108.5 GHz

To accurately estimate the gain of the antenna with the lens and the whole mm-wave circuitry, the output power of the MMIC must be known. However, in our case, the output power could not be directly measured for the particular MMIC sample mounted in the structure. The output power of −12.7 dBm was assumed based on the typical value of the other measured specimens (Fig. 2). With this assumption, the gain could be estimated from measured EIRP to be approximately 8.9 dBi. The ~13.6-dB difference between the gain and directivity indicates loss in the system. Such a high value could be attributed to several reasons. The most probable are the following:

- The output power of the specific MMIC used may be lower that assumed;
- Bond-wire interconnect might not be fully compensated by the matching circuit and could radiate some energy;
- The LTCC screen-printed circuit could contribute more significantly to the total loss than expected.

Some loss (roughly 1.5 dB) was caused by the reflection from the convex surface of the lens, which was not covered by an anti-reflective coating (calculated from reflection on boundary between free space and silicon). The intrinsic lens loss were considered to be less significant because the lens is made of high-resistivity silicon. Assuming 1 kΩcm resistivity of the silicon the losses in the lens is estimated to 0.05 dB at the frequency of 108.5 GHz on the basis of electromagnetic simulations. Considering that resistivity of high resistivity silicon is typically higher than 1 kΩcm, this effect is negligible.

IV. CONCLUSIONS

The AiP transmitter presented in this paper integrates components fabricated in different technologies. It operates above 100 GHz with peak EIRP of −3.8 dBm at 108.5 GHz. Its assembly is based on simple and popular methods and does not require complex machinery. The most advanced machine used for the assembly of the prototype described in this paper is a basic wire bonder that only supports thin wires infamous for poor performance at frequencies above 100 GHz. Therefore, its negative influence is alleviated to some extent by the matching circuit. Additionally, the losses in the wire bonds and microstrip lines are compensated by the silicon lens suspended over the antenna array, which narrows the beam and increases the EIRP. The lens performance is enhanced by attaching an impedance transformer, made of a microwave laminate, to its flat surface. The fixture that suspends the lens over the antenna array is straightforward and allows fine adjustment.

One of the main advantages of our design is that the assembly does not require sophisticated facilities. Although each main part (MMIC, LTCC board, and lens) is obtained from professional manufacturers, the integration is possible in a typical workshop of an electronic laboratory.

The other advantage is the modular construction of the device, which allows easy replacement and adjustment of components; for example, the lens can be replaced, and its suspension height can be fine-tuned.

Although the obtained EIRP is not as good as that of the other solutions that use an antenna fabricated on an LTCC substrate (Table II), our results show that a cost-effective mm-wave transmitter that operates above 100 GHz is feasible by utilizing the COTS components and commercially available technologies at the expense of performance. Nonetheless, room for further improvement is still available. For example, the efficiency can be increased by the addition of an anti-reflective coating to the convex surface of the lens, by shortening or elimination of bond-wire interconnections as well as by pinpointing and mitigating the losses in the LTCC structure.

REFERENCES

[1] Y. P. Zhang and D. Liu, "Antenna-on-Chip and Antenna-in-Package Solutions to Highly Integrated Millimeter-Wave Devices for Wireless Communications," in *IEEE Trans. Antennas Propag.*, vol. 57, no. 10, pp. 2830–2841, Oct. 2009. https://dx.doi.org/10.1109/TAP.2009.2029295

[2] D. Liu and Y. P. Zhang, "Integration of Array Antennas in Chip Package for 60-GHz Radios," *Proc. IEEE*, vol. 100, no. 7, pp. 2364–2371, Jul. 2012. https://dx.doi.org/10.1109/JPROC.2012.2186101

[3] T. Zwick, F. Boes, B. Göttel, A. Bhutani and M. Pauli, "Pea-Sized mmW Transceivers: QFN-Based Packaging Concepts for Millimeter-Wave Transceivers," in *IEEE Microw. Mag.*, vol. 18, no. 6, pp. 79–89, Sept.-Oct. 2017. https://dx.doi.org/10.1109/MMM.2017.2712020

[4] D. Dancila et al., "Differential microstrip patch antenna as feeder of a hyper-hemispherical lens for F-band MIMO radars," *Global Symposium on Millimeter Waves (GSMM) & ESA Workshop on Millimetre-Wave Technology and Applications*, Espoo, Finland, 2016, pp. 1–4. https://dx.doi.org/10.1109/GSMM.2016.7500312

[5] A. Bisognin et al., "Ball Grid Array Module With Integrated Shaped Lens for 5G Backhaul/Fronthaul Communications in F-Band," in *IEEE Trans. Antennas Propag.*, vol. 65, no. 12, pp. 6380–6394, Dec. 2017. https://dx.doi.org/10.1109/TAP.2017.2755439

[6] B. Goettel, W. Winkler, A. Bhutani, F. Boes, M. Pauli and T. Zwick, "Packaging Solution for a Millimeter-Wave System-on-Chip Radar," in *IEEE Trans. Compon. Packag. Manuf. Technol.*, vol. 8, no. 1, pp. 73–81, Jan. 2018. https://dx.doi.org/10.1109/TCPMT.2017.2758725

[7] M. Neshat, D. M. Hailu, M. Nezhad-Ahmadi, G. Z. Rafi and S. Safavi-Naeini, "Gain Measurement of Embedded On-Chip Antennas in mmW/THz Range," in *IEEE Trans. Antennas Propag.*, vol. 60, no. 5, pp. 2544–2549, May 2012. https://dx.doi.org/10.1109/TAP.2012.2189772

[8] R. Jain et al., "A 64-Pixel 0.42-THz Source SoC With Spatial Modulation Diversity for Computational Imaging," in *IEEE Journal of Solid-State Circuits*, vol. 55, no. 12, pp. 3281–3293, Dec. 2020. https://dx.doi.org/10.1109/JSSC.2020.3018819

[9] Y. Zhang and J. Mao, "An Overview of the Development of Antenna-in-Package Technology for Highly Integrated Wireless Devices," in *Proceedings of the IEEE*, vol. 107, no. 11, pp. 2265–2280, Nov. 2019. https://dx.doi.org/10.1109/JPROC.2019.2933267

[10] P. Hallbjorner, Z. He, S. Bruce and S. Cheng, "Low-Profile 77-GHz Lens Antenna With Array Feeder," in *IEEE Antennas Wireless Propag. Lett.*, vol. 11, pp. 205–207, 2012. https://dx.doi.org/10.1109/LAWP.2012.2188265

[11] S. Raman, N. S. Barker and G. M. Rebeiz, "A W-band dielectric-lens-based integrated monopulse radar receiver," in *IEEE Trans. Microw. Theory Techn.*, vol. 46, no. 12, pp. 2308–2316, Dec. 1998. https://dx.doi.org/10.1109/22.739216

[12] A. Dyck et al., "A Transmitter System-in-Package at 300 GHz With an Off-Chip Antenna and GaAs-Based MMICs," in *IEEE Transactions on Terahertz Science and Technology*, vol. 9, no. 3, pp. 335–344, May 2019. https://dx.doi.org/10.1109/TTHZ.2019.2910511

[13] Y. P. Zhang, M. Sun, and W. Lin, "Novel Antenna-in-Package Design in LTCC for Single-Chip RF Transceivers," *IEEE Trans. Antennas Propag.*, vol. 56, no. 7, pp. 2079–2088, Jul. 2008. https://dx.doi.org/10.1109/TAP.2008.924706

[14] T. Klein, M. Faassen, R. Kulke and C. Rusch, "A 77 GHz radar frontend in LTCC for small range, high precision industrial applications," *2012 7th European Microwave Integrated Circuit Conference*, Amsterdam, 2012, pp. 905–908.

[15] F. Bauer, X. Wang, W. Menzel and A. Stelzer, "A 79-GHz Radar Sensor in LTCC Technology Using Grid Array Antennas," in *IEEE Transactions on Microwave Theory and Techniques*, vol. 61, no. 6, pp. 2514–2521, June 2013. https://dx.doi.org/10.1109/TMTT.2013.2260766

[16] F. Sickinger et al., "Automotive Satellite Radar Sensor System based on an LTCC Miniature Frontend," *2018 IEEE MTT-S International Conference on Microwaves for Intelligent Mobility (ICMIM)*, Munich, 2018, pp. 1–4. https://dx.doi.org/10.1109/ICMIM.2018.8443535

[17] X. Wang and A. Stelzer, "A 79-GHz LTCC RF-frontend for short-range applications," *2011 IEEE MTT-S International Microwave Symposium*, Baltimore, MD, 2011, pp. 1–4. https://dx.doi.org/10.1109/MWSYM.2011.5972679

[18] X. Wang, C. Yu, D. Qin and W. Lu, "W-Band High-Gain Substrate Integrated Cavity Antenna Array on LTCC," in *IEEE Transactions on Antennas and Propagation*, vol. 67, no. 11, pp. 6883–6893, Nov. 2019. https://dx.doi.org/10.1109/TAP.2019.2927896

[19] S. Beer, L. Pires, C. Rusch, J. Paaso and T. Zwick, "A 122 GHz Microstrip Slot Antenna with via-fence resonator in LTCC technology," *6th Europ. Conf. Antennas Propag. (EUCAP)*, Prague, Czech Republic, 2012, pp. 1329–1332. https://dx.doi.org/10.1109/EuCAP.2012.6205894

[20] P. Piasecki, Y. Yashchyshyn, "Study of D-band LTCC Leaky Wave Antenna Optimized for Broadside Radiation," *Radioengineering*, vol. 27, no. 2, pp. 463-468, June 2018. https://dx.doi.org/10.13164/re.2018.0463

[21] J. Xiao, X. Li, Z. Qi and H. Zhu, "140-GHz TE_{340}-Mode Substrate Integrated Cavities-Fed Slot Antenna Array in LTCC," in *IEEE Access*, vol. 7, pp. 26307–26313, 2019. https://dx.doi.org/10.1109/ACCESS.2019.2900989

[22] M. Henry et al., "Integrated air-filled waveguide antennas in LTCC for G-band operation," *2008 Asia-Pacific Microwave Conference*, Macau, 2008, pp. 1–4. https://dx.doi.org/10.1109/APMC.2008.4957967

[23] J. Xu, Z. N. Chen and X. Qing, "270-GHz LTCC-Integrated Strip-Loaded Linearly Polarized Radial Line Slot Array Antenna," in *IEEE Transactions on Antennas and Propagation*, vol. 61, no. 4, pp. 1794–1801, April 2013. https://dx.doi.org/10.1109/TAP.2012.2237007

[24] T. Tajima, H. Song, K. Ajito, M. Yaita and N. Kukutsu, "300-GHz Step-Profiled Corrugated Horn Antennas Integrated in LTCC," in *IEEE Transactions on Antennas and Propagation*, vol. 62, no. 11, pp. 5437–5444, Nov. 2014. https://dx.doi.org/10.1109/TAP.2014.2350520

[25] M. Lahti, K. Kautio, M. Karppinen, K. Keränen, J. Ollila, and P. Karioja, "Review of LTCC Technology for Millimeter Waves and Photonics", *International Journal of Electronics and Telecommunications*, 2020, vol. 66 no. 2, pp. 361-367. https://dx.doi.org/10.24425/ijet.2020.131886

[26] S. Beer and T. Zwick, "122 GHz antenna-integration in a plastic package based on a flip chip interconnect," *2011 IEEE MTT-S International Microwave Workshop Series on Millimeter Wave Integration Technologies*, Sitges, 2011, pp. 37–40. https://dx.doi.org/10.1109/IMWS3.2011.6061881

[27] R. Shireen, S. Shi, P. Yao and D. W. Prather, "Multi-Chip Module Packaging For W-Band $LiNbO_3$ Modulator," in *IEEE Microwave and Wireless Components Letters*, vol. 21, no. 3, pp. 145–147, March 2011. https://dx.doi.org/10.1109/LMWC.2010.2103375

[28] V. Valenta, T. Spreng, S. Yuan, W. Winkler, V. Ziegler, D. Dancila, A. Rydberg, and H. Schumacher, "Design and experimental evaluation of compensated bondwire interconnects above 100 GHz," *International Journal of Microwave and Wireless Technologies*, vol. 7, no. 3-4, pp. 261–270, 2015. https://dx.doi.org/10.1017/S1759078715000070

[29] A. Bhutani, B. Göttel, A. Lipp and T. Zwick, "Packaging Solution Based on Low-Temperature Cofired Ceramic Technology for Frequencies Beyond 100 GHz," in *IEEE Transactions on Components, Packaging and Manufacturing Technology*, vol. 9, no. 5, pp. 945–954, May 2019. https://dx.doi.org/10.1109/TCPMT.2018.2882062

[30] L. Wu, S. Liao and Q. Xue, "A 312-GHz CMOS Injection-Locked Radiator With Chip-and-Package Distributed Antenna," in *IEEE Journal of Solid-State Circuits*, vol. 52, no. 11, pp. 2920–2933, Nov. 2017. https://dx.doi.org/10.1109/JSSC.2017.2727046

[31] Z. Tong, A. Fischer, A. Stelzer and L. Maurer, "Radiation Performance Enhancement of E-Band Antenna in Package," in *IEEE Trans. Compon. Packag. Manuf. Technol.*, vol. 3, no. 11, pp. 1953–1959, Nov. 2013. https://dx.doi.org/10.1109/TCPMT.2013.2272039

[32] P. Bajurko et al., "A 110 GHz Hybrid Integrated Transmitter Design," *2020 23rd International Microwave and Radar Conference (MIKON)*, Warsaw, Poland, 2020, pp. 367–370. https://dx.doi.org/10.23919/MIKON48703.2020.9253943

[33] P. R. Bajurko, "Millimeter wave permittivity and loss tangent measurements of LTCC materials," *2016 21st International Conference on Microwave, Radar and Wireless Communications (MIKON)*, Krakow, 2016, pp. 1–4. https://dx.doi.org/10.1109/MIKON.2016.7492104

[34] Y. Yashchyshyn et al. , "Experience in developing LTCC technologies for mm-Wave antennas," *11th Eur. Conf. Antennas Propag. (EUCAP)*, Paris, France, 2017. https://dx.doi.org/10.23919/EuCAP.2017.792808

[35] J. Sobolewski and P. R. Bajurko, "Design of LTCC patch antenna for increased bandwidth and reduced susceptibility to fabrication process

inaccuracies," *22nd Int. Microw. Radar Conf. (MIKON)*, Poznan, Poland, 2018, pp. 218–221. https://dx.doi.org/10.23919/MIKON.2018.8405182

[36] C. A. Balanis, *Antenna theory: analysis and design*, John Wiley & Sons 2016, chapter 2, section 6 "Directivity".

[37] H. Y. Kim et al., "A 60 GHz LTCC antenna in package with low power CMOS radio," *Asia-Pacific Microw. Conf. Proc. (APMC)*, Seoul, Republic of Korea, 2013, pp. 155–157. https://dx.doi.org/10.1109/APMC.2013.6695222

[38] P. Pursula et al., "60-GHz Millimeter-Wave Identification Reader on 90-nm CMOS and LTCC," in *IEEE Trans. Microw. Theory Techn.*, vol. 59, no. 4, pp. 1166–1173, April 2011. https://dx.doi.org/10.1109/TMTT.2011.2114200

[39] A. Vahdati et al., "90 GHz CMOS Phased-Array Transmitter Integrated on LTCC," in *IEEE Trans. Antennas Propag.*, vol. 65, no. 12, pp. 6363–6371, Dec. 2017. https://dx.doi.org/10.1109/TAP.2017.2743009